Applied Physics Letters

Epitaxial growth and thermoelectric properties of Mg_3Bi_2 thin films deposited by magnetron sputtering

Cite as: Appl. Phys. Lett. **120**, 051901 (2022); https://doi.org/10.1063/5.0074419
Submitted: 08 October 2021 • Accepted: 13 January 2022 • Published Online: 04 February 2022

Grzegorz Sadowski, Yongbin Zhu, Rui Shu, et al.

Applied Physics Letters ARTICLE scitation.org/journal/apl

Epitaxial growth and thermoelectric properties of Mg_3Bi_2 thin films deposited by magnetron sputtering

Cite as: Appl. Phys. Lett. **120**, 051901 (2022); doi: 10.1063/5.0074419
Submitted: 8 October 2021 · Accepted: 13 January 2022 ·
Published Online: 4 February 2022

View Online Export Citation CrossMark

Grzegorz Sadowski,[1,2] Yongbin Zhu,[3] Rui Shu,[1] Tao Feng,[3] Arnaud le Febvrier,[1] Denis Music,[2] Weishu Liu,[3,4,a)] and Per Eklund[1,a)]

AFFILIATIONS

[1]Thin Film Physics Division, Department of Physics, Chemistry, and Biology (IFM), Linköping University, Linköping SE-581 83, Sweden
[2]Department of Materials Science and Applied Mathematics, Malmö University, Malmö SE-205 06, Sweden
[3]Department of Materials Science and Engineering, Southern University of Science and Technology, Shenzhen, Guangdong 518055, China
[4]Guangdong Provincial Key Laboratory of Functional Oxide Materials and Devices, Southern University of Science and Technology, Shenzhen, Guangdong 518055, China

Note: This paper is part of the APL Special Collection on Thermoelectric Materials Science and Technology Towards Applications.
[a)]**Authors to whom correspondence should be addressed:** liuws@sustech.edu.cn and per.eklund@liu.se

ABSTRACT

Mg_3Sb_2-based thermoelectric materials attract attention for applications near room temperature. Here, Mg-Bi films were synthesized using magnetron sputtering at deposition temperatures from room temperature to 400 °C. Single-phase Mg_3Bi_2 thin films were grown on *c*-plane-oriented sapphire and Si(100) substrates at a low deposition temperature of 200 °C. The Mg_3Bi_2 films grew epitaxially on *c*-sapphire and fiber-textured on Si(100). The orientation relationships for the Mg_3Bi_2 film with respect to the *c*-sapphire substrate are (0001) Mg_3Bi_2||(0001) Al_2O_3 and [11$\bar{2}$0] Mg_3Bi_2||[11$\bar{2}$0] Al_2O_3. The observed epitaxy is consistent with the relatively high work of separation, calculated by the density functional theory, of 6.92 J m^{-2} for the Mg_3Bi_2 (0001)/Al_2O_3 (0001) interface. Mg_3Bi_2 films exhibited an in-plane electrical resistivity of 34 $\mu\Omega$ m and a Seebeck coefficient of +82.5 μV K^{-1}, yielding a thermoelectric power factor of 200 μW m^{-1} K^{-2} near room temperature.

Thermoelectric thin films are desired for microscale devices using semiconductor coolers[1] or self-powered systems for sensors and the Internet of Things.[2,3] The interest in thermoelectric thin films is also largely driven by possible improvement in thermoelectric properties, for example, in lower dimensional structures due to quantum confinement[4] and phonon-scattering effects.[5] Compared with bulk materials, thermoelectric thin films, especially single-crystal thin films, are attractive for assembling micro-thermoelectric generators.[2,3]

Conventional thermoelectric materials, most notably Bi_2Te_3-based ones, have some well-known disadvantages in that they are brittle and contain the extremely scarce element Te. The Zintl phase Mg_3Bi_2 and its alloys in a La_2O_3-type trigonal structure have received attention because of their nontoxicity, high elemental abundancy, and good thermoelectric properties for energy harvesting applications.[6–15] For example, an average thermoelectric figure of merit of polycrystalline $Mg_{3+\delta}Sb_xBi_{2-x}$ has been reported to be comparable with that of the conventional *n*-type $Bi_2Te_{2.7}Se_{0.3}$ in the temperature range of 50–250 °C.[10] Further studies have focused on the improvement of thermoelectric properties near room temperature.[1,11,12,14,16,17] Single-crystal Mg_3Bi_2 and its alloys were synthesized by the Mg-flux method.[8,13] For vacuum-based thin-film deposition, the relatively high vapor pressure of Mg (of the order of 10^{-6} mbar at 250 °C and 10^{-4} mbar at 330 °C)[18] makes it challenging to synthesize pure Mg_3Bi_2 thin films at high temperatures. Matsui *et al.* reported growing polycrystalline Mg_3Bi_2 thin films on a copper plate at 200 °C by radio frequency magnetron sputtering.[19] Single-crystalline Mg_3Bi_2 thin films deposited using molecular beam epitaxy have been reported.[20,21] However, none of the above studies were aiming for thermoelectric applications.

The growth of epitaxial thin films is, therefore, important to enable characterization and explanation of the fundamental physical properties of Mg_3Bi_2-based thin films. Here, we grow a Mg_3Bi_2 thin film on *c*- and *r*-plane-oriented sapphire and Si(100) substrates by magnetron co-sputtering of Mg and Bi targets. Epitaxial single-phase Mg_3Bi_2 is synthesized on the *c*-sapphire substrate, and a fiber-textured Mg_3Bi_2 film on Si(100) substrates. The orientation relationships for Mg_3Bi_2 with respect to the *c*-sapphire substrate are: (0001) Mg_3Bi_2||(0001) Al_2O_3 and [11$\bar{2}$0] Mg_3Bi_2||[1$\bar{1}$20] Al_2O_3. Moreover, the in-plane thermoelectric properties of the Mg_3Bi_2 films grown on *c*-sapphire were measured from room temperature to deposition temperatures.

Mg_3Bi_2 films were deposited using direct current (*dc*) magnetron sputtering in an ultrahigh vacuum chamber (base pressure $< 4 \times 10^{-6}$ Pa). The deposition system is described elsewhere.[22] Mg and Bi circular targets (50 mm in diameter) were used and driven by *dc*-power supplies with optimized (i.e., yielding approximately the desired 3:2 composition; see the supplementary material, Fig. S1) power of 90 and 15 W, respectively. The Ar gas flow rate was fixed to 80 sccm corresponding to a working pressure of 0.5 Pa. The substrate holder was maintained at different temperatures from non-intentional heating ("room temperature," RT) to 400 °C, rotated at 15 rpm, with the substrates electrically floating. The films were deposited on Si(100) and *c*- and *r*-plane-oriented sapphire substrates. The films deposited on Si(100) and *c*-sapphire substrates were used for microstructural characterization by x-ray diffraction (XRD) and elemental composition determined by energy-dispersive x-ray spectrometry (EDS). The electrical resistivity ρ, the Seebeck coefficient S, and the power factor S^2/ρ of films on *c*- and *r*-sapphire were measured by a commercial system (CTA-3, Cryoall Co., Ltd., China) under a low-pressure helium atmosphere from RT to 200 °C (growth temperature). The uncertainty for thermoelectric property measurements is around 5%. The Hall coefficient R_H for Mg_3Bi_2 grown on c-sapphire was obtained from the magnetic field-dependent Hall resistivities using the electrical transport option in a quantum design physical property measurement system (PPMS). The charge carrier concentration n_H was calculated by $n_H = 1/eR_H$. The work of separation[23] was calculated at 0 K for the interface of interest using the density functional theory (DFT) as implemented in the Vienna *ab initio* simulation package (VASP).[24–26] The generalized gradient approximation was employed in VASP and parametrized by Perdew, Burke, and Ernzerhof.[27] The precision and convergence for the interface were specified by a reciprocal *k*-grid of 5 × 5 × 1, 520 eV cutoff, and 0.01 meV criterion for the total energy. Full structural optimization was made by minimizing the interatomic forces and optimizing the lattice parameters.

Figure 1 shows XRD patterns of as-deposited Mg-Bi films on *c*-sapphire and Si(100) with T_s varied from RT to 400 °C. The elevated growth temperature improved the crystallinity of Mg-Bi films on both substrates. For the films deposited on *c*-sapphire, the peaks of the Mg-Bi film deposited at RT can be attributed to the polycrystalline Mg_3Bi_2 phase. When increasing T_s to 200 °C, a 0001 peak of Mg_3Bi_2 shows up at 11.9°, and the intensities of corresponding higher-order 000*l* peaks increase, indicating the possibility of epitaxial growth. Films deposited at higher T_s have clearer, sharper peaks corresponding to Mg_3Bi_2, but also exhibit an additional peak located at 27.0°, which can be attributed to the 01$\bar{1}$2 peak of Bi. The presence of metallic Bi is correlated with Mg deficiency for deposition at higher temperatures ($T_s \geq 300$ °C, see the supplementary material, Fig. S1). The films grown on Si(100) at $T_s \leq 200$ °C show the same Mg_3Bi_2 phase with similar orientations with films grown on *c*-sapphire, while the films grown with $T_s > 200$ °C exhibit 11$\bar{2}$2, 11$\bar{2}$3, 10$\bar{1}$5, and 12$\bar{3}$4 peaks of substantial intensity, indicating the presence of other orientations. Therefore, $T_s = 200$ °C is an optimal temperature, sufficient to grow single-phase Mg_3Bi_2 on both substrates, which is in agreement with the previous work[28] on the synthesis of Mg_3Bi_2 films using radio frequency magnetron sputtering.

To further identify the crystallographic relationship between Mg_3Bi_2 films and substrates, pole figures of (0001) and (11$\bar{2}$2) planes were acquired for Mg_3Bi_2 films grown at $T_s = 200$ °C on *c*-sapphire and Si(100) substrates, as shown in Fig. 2. The pole figure of the 0001

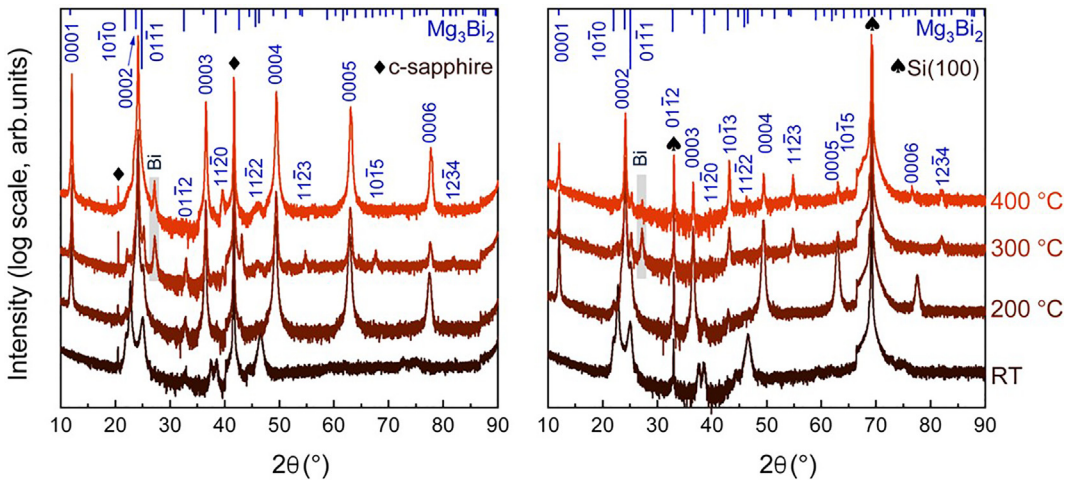

FIG. 1. X-ray diffraction patterns of Mg_3Bi_2 thin films grown on *c*-sapphire and Si(100) at different temperatures. The peak position of the Mg_3Bi_2 phase is from powder diffraction file No. 65-8732.

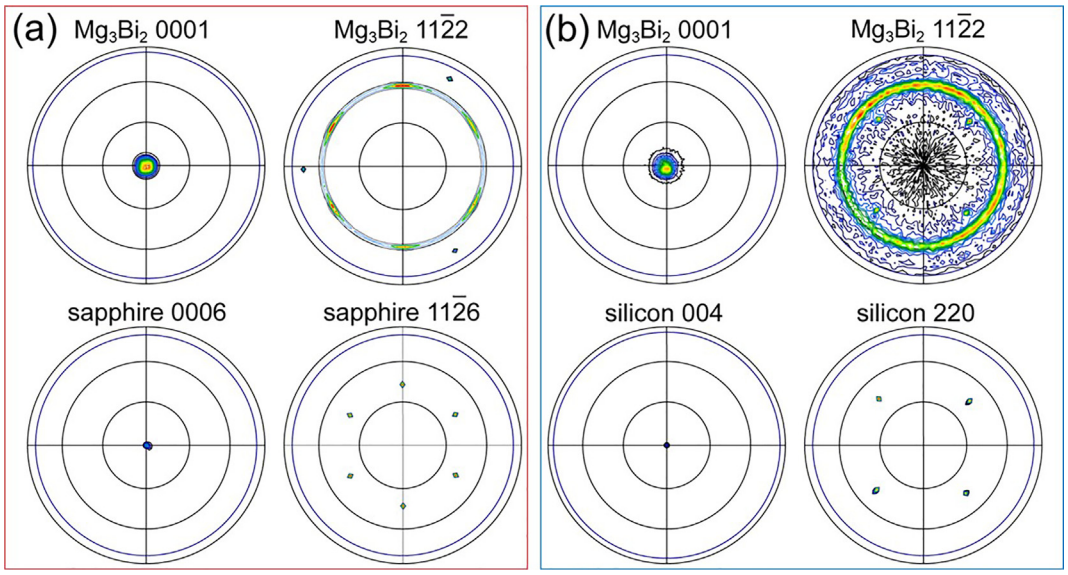

FIG. 2. 0001 and 11$\bar{2}$2 pole figures of Mg_3Bi_2 thin films deposited at 200 °C on the *c*-sapphire substrate (a) and Si(100) substrate (b), and corresponding pole figure 0006 and 11$\bar{2}$6 of c-sapphire, 004 and 220 of the silicon substrate.

peak [Fig. 2(a), top left] shows diffraction only at the center (i.e., tilt-angle $\chi = 0$) consistent with basal-plane orientation [Fig. 2(a), bottom left]. The 11$\bar{2}$2 pole figure [Fig. 2(a), top left] shows a set of sixfold symmetric spots out of a visible ring at $\chi = 57.5°$, corresponding to the angle between (000*l*) and (11$\bar{2}$2) planes in the trigonal Mg_3Bi_2 structure. Their in-plane rotation angles φ are matched with the same diffraction peaks of the 11$\bar{2}$6 peak of Al_2O_3, consistent with the φ scans (the supplementary material, Fig. S2), indicating that Mg_3Bi_2 (11$\bar{2}$2) planes have the same in-plane orientation as Al_2O_3 (11$\bar{2}$6). We also find a set of threefold symmetric diffraction peaks at $\chi = 72.4°$, originating from the (20$\bar{2}$2) plane of sapphire. Based on these results, we conclude that the orientation relationships for the Mg_3Bi_2 film with respect to the *c*-sapphire substrate are: (0001) Mg_3Bi_2||(0001) Al_2O_3 and [11$\bar{2}$0] Mg_3Bi_2||[11$\bar{2}$0] Al_2O_3. In comparison, the 0001 and 11$\bar{2}$2 pole figures of Mg_3Bi_2 films grown on Si(100) are shown in Fig. 2(b), top. The 0001 pole figure shows diffraction only at the center, whereas the 11$\bar{2}$2 pole figure exhibits a broad ring of uniform intensity, indicating that the majority of grains grow in the same direction out of the plane but are randomly distributed in all directions in-plane, i.e., fiber texture.

To rationalize the epitaxy of Mg_3Bi_2 on sapphire, the interface structure is analyzed. A graphical in-plane view of the interface is shown in Fig. 3(a). The symmetries of the two lattices are close to each other, as confirmed by the in-plane mismatch value of 1.7% between Mg_3Bi_2 and Al_2O_3.[21] To quantify the interfacial strength, the work of separation was calculated by DFT, as illustrated in Fig. 3(b). A mixture of covalent and ionic bonding between Mg and O as well as Bi and O across the interface, each being threefold coordinated, is observed, implying strong bonding. The work of separation increases, while the interface energy decreases.[29] The work of separation of 6.92 J m^{-2} was obtained for the Mg_3Bi_2 (0001)/Al_2O_3 (0001) interface, which is sufficiently strong to facilitate epitaxial growth in comparison with Cu (111)/Al_2O_3 (0001)[30] and V_2AlC (0001)/Al_2O_3 (11$\bar{2}$0),[31] having the work of separation of 5.48 and 2.86 J m^{-2}, respectively. However, this work of separation is also weaker than 12.70 J m^{-2} for Nb (111)/Al_2O_3 (0001)[32] and 9.31 J m^{-2} for the TiO_2 (100)/Al_2O_3 (0001) interface.[33] It may lead to the epitaxial quality of Mg_3Bi_2 on sapphire not being as good as expected with some random reflections observed from Mg_3Bi_2 in the XRD pattern [Fig. 1(a)] and a visible ring in pole figures [Fig. 2(a)].

Figure 4 shows the temperature-dependent thermoelectric properties of the single-phase Mg_3Bi_2 films deposited on *c*- and *r*-sapphire (both having the same crystalline feature, Fig. S3). The electrical resistivity ρ of the Mg_3Bi_2 film is essentially constant with a variation from 34.5 to 36.8 $\mu\Omega$ m (i.e., within error margins) in the measured temperature range between 30 and 200 °C. These obtained values of the resistivity are consistent with the range expected for the semimetal Mg_3Bi_2 with a small band overlap energy at room temperature.[11,34] The Mg_3Bi_2 film exhibits *p*-type behavior and a linearly decreasing Seebeck coefficient from +82.5 to +53.4 μV K^{-1} when temperature increases from RT to 200 °C. The power factor (S^2/ρ) of the Mg_3Bi_2 film is 197 at 30 °C and 79 μW m^{-1} K^{-2} at 200 °C. A comparison of thermoelectric properties at 30 °C between the epitaxial Mg_3Bi_2 film in this work and reported values for single-crystal and bulk Mg_3Bi_2 materials is shown in the supplementary material, Table S1. There is a significant difference in the electrical resistivity due to anisotropy and the synthesis methods.[13,35] Generally, the in-plane resistivity is higher than that of out-of-plane. The in-plane resistivity of the Mg_3Bi_2 thin film in this work is 34–36 $\mu\Omega$ m. Kim *et al.*[36] found a large anisotropy in Mg_3Bi_2 single crystals. Xin *et al.*[8] recently showed that the out-of-plane resistivity (along the *c* axis) is only half of the out-of-plane one (along the *b* axis) in the temperature range 2–320 K. There are also differences in the measured resistivity of bulk polycrystalline Mg_3Bi_2 compounds prepared by mechanical alloying[37] and by solid-state reaction.[38] Therefore, the synthesis methods play a role in determining the impurity content, grain sizes, and composition, significantly affecting

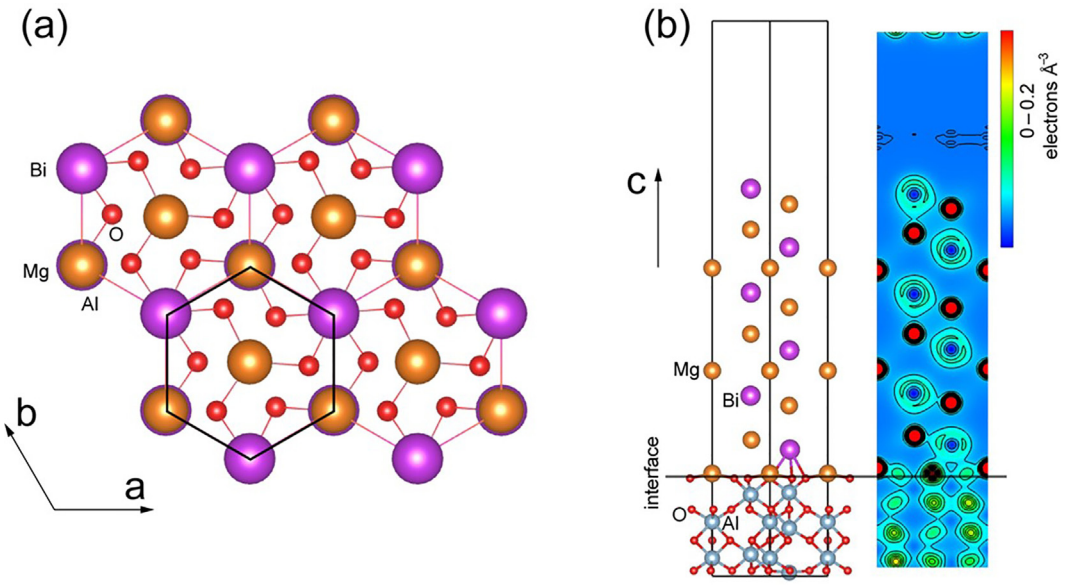

FIG. 3. (a) Ball-stick model of Mg_3Bi_2 (0001) on O-terminated sapphire as an in-plane view. (b) Structural model of the Mg_3Bi_2/Al_2O_3 interface together with a corresponding electron density distribution.

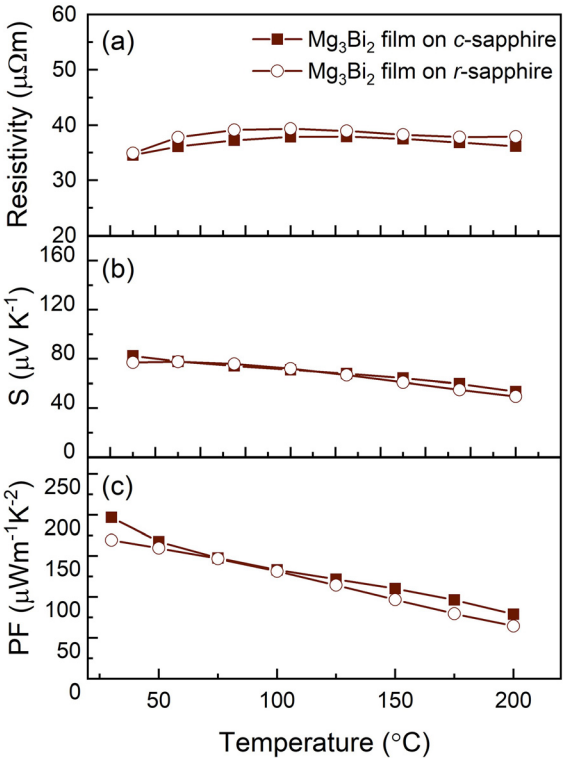

FIG. 4. Thermoelectric properties of the Mg_3Bi_2 thin film deposited at 200 °C on *c*-sapphire (filled box) and *r*-sapphire (empty circle): electrical resistivity ρ, Seebeck coefficient (S), and power factor S^2/ρ (PF) as a function of temperature.

electrical transport. Also, the Mg_3Bi_2 materials mentioned above are all *p*-type semiconductors. However, with Mg overstoichiometry and Te doping,[11] this phase may turn to *n*-type. The crystalline quality and the presence of dopants can also affect the carrier concentration (n_H) and mobility (μ_H). In our case (Fig. S4), n_H of the Mg_3Bi_2 film grown on *c*-sapphire was $\sim 1.7 \times 10^{19}$ cm^{-3} at 2 K and slightly increased to 4.0×10^{19} cm^{-3} at 300 K. These values are in good agreement with earlier reports[8,11,39] (several tens of 10^{19} cm^{-3}). The μ_H decreased from 59.1 to 14.0 cm^2 V^{-1} s^{-1} when the temperature increased from 2 to 300 K. This trend is generally due to more frequent carrier-scattering by phonons at higher temperatures. Compared to previous results on the $Mg_{3.2}Bi_2$ single-crystal bulk[8] and the Mg_3Bi_2 film grown by molecular beam epitaxy,[39] μ_H of the Mg_3Bi_2 film in this work is dropping significantly earlier, above 10 K, which may be due to predominant grain-boundary scattering. The behavior of μ_H of n_H indicates a semimetallic characteristic and can be influenced by crystalline quality, in turn affecting defect scattering of charge carriers. As temperature increases above room temperature, n_H increases sharply (which is favorable for high S and low ρ) while μ_H decreases (favorable for low S and high ρ); the resistivity increases (which is usual for semimetals) while the Seebeck coefficient decreases. The sharp increase in the carrier concentration with temperature could be a sign of the bipolar effect,[40] which is common in semimetals and narrow-gap semiconductors. The bipolar effect is detrimental to the Seebeck effect.[41] A decreasing bipolar effect can be achieved through increasing the majority carrier concentration, for example, through doping, and decreasing the minority carrier concentration.[42]

In conclusion, we have demonstrated that single-phase Mg_3Bi_2 thin films can be grown on different substrates at a low deposition temperature of 200 °C. The Mg_3Bi_2 films grew epitaxially on *c*-sapphire and fiber-textured on Si(100) substrates. The orientation

relationships for the Mg_3Bi_2 film with respect to the *c*-sapphire substrate are (0001) Mg_3Bi_2||(0001) Al_2O_3 and [11$\bar{2}$0] Mg_3Bi_2||[11$\bar{2}$0] Al_2O_3. The observed epitaxy is consistent with the relatively high work of separation, calculated by DFT, of 6.92 J m^{-2} obtained for the Mg_3Bi_2 (0001)/Al_2O_3 (0001) interface. The in-plane thermoelectric properties of the Mg_3Bi_2 films grown on *c*-sapphire were measured from room temperature to 200 °C. The in-plane resistivity of Mg_3Bi_2 films is 34 $\mu\Omega$m near room temperature, and the Seebeck coefficient linearly decreases from 82.5 to 53.4 μV K^{-1} from room temperature to 200 °C. The power factor is about 200 μWm^{-1} K^{-2} near room temperature. The work has prospects for preparing Mg_3Bi_2-based thin-film thermoelectrics applied near room temperature and future thermoelectric property improvement for Mg_3Bi_2 through doping.

See the supplementary material for additional XRD and composition data, comparison of thermoelectric properties, Hall carrier concentration, and carrier mobility.

This work was supported financially by the Swedish Government Strategic Research Area in Materials Science on Functional Materials at Linköping University (Faculty Grant SFO-Mat-LiU No. 2009 00971), the Knut and Alice Wallenberg Foundation through the Wallenberg Academy Fellows program (No. KAW-2020.0196), the Swedish Research Council (VR) under Project Nos. 2016-03365 and 2021-03826, the National Key Research and Development Program of China under Grant No. 2018YFB0703600, the National Natural Science Foundation of China under Grant No. 51872133, the Guangdong Innovative and Entrepreneurial Research Team Program under Grant No. 2016ZT06G587, and the Tencent Foundation through the XPLORER PRIZE, Guangdong Provincial Key Laboratory Program (No. 2021B1212040001) from the Department of Science and Technology of Guangdong Province. The computations were performed on resources provided by the Swedish National Infrastructure for Computing (SNIC) at National Supercomputer Centre (NSC) partially funded by the Swedish Research Council through Grant Agreement No. 2018-05973.

AUTHOR DECLARATIONS

Conflict of Interest

The authors have no conflicts to disclose.

Author Contributions

R.S. and P.E. initiated the study. P.E., W.L. and A.l.F. supervised the research. G.S. and R.S. planned and performed the sample synthesis and microstructure characterization with contributions from A.l.F., and P.E., G.S, and Y.Z. performed and analyzed thermoelectric property measurements. T.F. performed and analyzed the Hall measurements. D.M. performed DFT calculations and wrote the corresponding part of the manuscript. G.S., R.S., and P.E. wrote the manuscript with contributions from the co-authors. All co-authors read, edited, and commented on successive version of the manuscript.

DATA AVAILABILITY

The data that support the findings of this study are available within the article and its supplementary material or are available from the corresponding authors upon reasonable request.

REFERENCES

[1]I. Chowdhury, R. Prasher, K. Lofgreen, G. Chrysler, S. Narasimhan, R. Mahajan, D. Koester, R. Alley, and R. Venkatasubramanian, Nat. Nanotechnol. **4**, 235 (2009).
[2]Y. Du, J. Xu, B. Paul, and P. Eklund, Appl. Mater. Today **12**, 366 (2018).
[3]W. Liu, J. Hu, S. Zhang, M. Deng, C.-G. Han, and Y. Liu, Mater. Today Phys. **1**, 50 (2017).
[4]L. D. Hicks, T. C. Harman, X. Sun, and M. S. Dresselhaus, Phys. Rev. B **53**, R10493 (1996).
[5]R. Venkatasubramanian, E. Siivola, T. Colpitts, and B. O'Quinn, Nature **413**, 597 (2001).
[6]H. Tamaki, H. K. Sato, and T. Kanno, Adv. Mater. **28**, 10182 (2016).
[7]J. Zhang, L. Song, S. H. Pedersen, H. Yin, L. T. Hung, and B. B. Iversen, Nat. Commun. **8**, 13901 (2017).
[8]J. Xin, G. Li, G. Auffermann, H. Borrmann, W. Schnelle, J. Gooth, X. Zhao, T. Zhu, C. Felser, and C. Fu, Mater. Today Phys. **7**, 61 (2018).
[9]K. Imasato, S. Ohno, S. D. Kang, and G. J. Snyder, APL Mater. **6**, 016106 (2018).
[10]R. Shu, Y. Zhou, Q. Wang, Z. Han, Y. Zhu, Y. Liu, Y. Chen, M. Gu, W. Xu, Y. Wang, W. Zhang, L. Huang, and W. Liu, Adv. Funct. Mater. **29**, 1807235 (2019).
[11]J. Mao, H. Zhu, Z. Ding, Z. Liu, G. A. Gamage, G. Chen, and Z. Ren, Science **365**, 495 (2019).
[12]X. Shi, C. Sun, Z. Bu, X. Zhang, Y. Wu, S. Lin, W. Li, A. Faghaninia, A. Jain, and Y. Pei, Adv. Sci. **6**, 1802286 (2019).
[13]Y. Pan, M. Yao, X. Hong, Y. Zhu, F. Fan, K. Imasato, Y. He, C. Hess, J. Fink, J. Yang, B. Büchner, C. Fu, G. J. Snyder, and C. Felser, Energy Environ. Sci. **13**, 1717 (2020).
[14]Z. Han, J.-W. Li, F. Jiang, J. Xia, B.-P. Zhang, J.-F. Li, and W. Liu, "Room-temperature thermoelectric materials: Challenges and a new paradigm," J. Materiomics (published online 2021).
[15]R. Shu, Z. Han, A. Elsukova, Y. Zhu, P. Qin, F. Jiang, J. Lu, P. O. Å. Persson, J. Palisaitis, A. le Febvrier, W. Zhang, O. Cojocaru-Mirédin, Y. Yu, P. Eklund, and W. Liu, arXiv:2107.09397 Cond-Mat (2021).
[16]Z. Han, Z. Gui, Y. B. Zhu, P. Qin, B.-P. Zhang, W. Zhang, L. Huang, and W. Liu, Research **2020**, 1672051.
[17]K. Imasato, S. Dongmin Kang, and G. Jeffrey Snyder, Energy Environ. Sci. **12**, 965 (2019).
[18]W. Gilbreath, *The Vapor Pressure of Magnesium between 223 and 385 C* (National Aeronautics and Space Administration, Washington, DC, 1965).
[19]M. Matsui, H. Kuwata, D. Mori, N. Imanishi, and M. Mizuhata, Front. Chem. **7**, 7 (2019).
[20]M. Tong, Y. Hu, X. Xie, X. Zhu, Z. Wang, X. Cheng, and T. Jiang, Opto-Electron. Adv. **3**, 200023 (2020).
[21]T. Zhou, M. Tong, Y. Zhang, X. Xie, Z.-Y. Wang, T. Jiang, X.-G. Zhu, and X.-C. Lai, Phys. Rev. B **103**, 125405 (2021).
[22]A. le Febvrier, L. Landälv, T. Liersch, D. Sandmark, P. Sandström, and P. Eklund, Vacuum **187**, 110137 (2021).
[23]Z. Lin and P. D. Bristowe, Phys. Rev. B **75**, 205423 (2007).
[24]G. Kresse and J. Hafner, Phys. Rev. B **48**, 13115 (1993).
[25]G. Kresse and J. Hafner, Phys. Rev. B **49**, 14251 (1994).
[26]G. Kresse and D. Joubert, Phys. Rev. B **59**, 1758 (1999).
[27]J. P. Perdew, K. Burke, and M. Ernzerhof, Phys. Rev. Lett. **77**, 3865 (1996).
[28]H. Kuwata, M. Matsui, and N. Imanishi, ECS Meet. Abstr. **MA2016-02**, 686 (2016).
[29]H. Guo, Y. Qi, and X. Li, J. Appl. Phys. **107**, 033722 (2010).
[30]F. Herrig, D. Music, B. Völker, M. Hans, P. J. Pöllmann, A. L. Ravensburg, and J. M. Schneider, Metals **8**, 384 (2018).
[31]D. P. Sigumonrong, J. Zhang, Y. Zhou, D. Music, J. Emmerlich, J. Mayer, and J. M. Schneider, Scr. Mater. **64**, 347 (2011).
[32]I. G. Batirev, A. Alavi, M. W. Finnis, and T. Deutsch, Phys. Rev. Lett. **82**, 1510 (1999).
[33]M. N. Popov, J. Spitaler, M. Mühlbacher, C. Walter, J. Keckes, C. Mitterer, and C. Draxl, Phys. Rev. B **86**, 205309 (2012).

[34]H. Shang, Z. Liang, C. Xu, J. Mao, H. Gu, F. Ding, and Z. Ren, Research **2020**, 1219461.
[35]A. Li, C. Fu, X. Zhao, and T. Zhu, "High-performance Mg_3Sb_2-xBi_x thermoelectrics: Progress and perspective," Research (Wash. DC), 1934848 (2020).
[36]S. H. Kim, C. M. Kim, Y.-K. Hong, K. I. Sim, J. H. Kim, T. Onimaru, T. Takabatake, and M.-H. Jung, Mater. Res. Express **2**, 055903 (2015).
[37]H. X. Xin and X. Y. Qin, J. Phys. Appl. Phys. **39**, 5331 (2006).
[38]V. Ponnambalam and D. T. Morelli, J. Electron. Mater. **42**, 1307 (2013).
[39]T. Zhou, M. Tong, X. Xie, Y. Yu, X. Zhu, Z.-Y. Wang, and T. Jiang, J. Phys. Chem. Lett. **11**, 6475 (2020).
[40]J. J. Gong, A. J. Hong, J. Shuai, L. Li, Z. B. Yan, Z. F. Ren, and J.-M. Liu, Phys. Chem. Chem. Phys. **18**, 16566 (2016).
[41]Z. Chen, X. Zhang, J. Ren, Z. Zeng, Y. Chen, J. He, L. Chen, and Y. Pei, Nat. Commun. **12**, 3837 (2021).
[42]Z. Liu, J. Mao, S. Peng, B. Zhou, W. Gao, J. Sui, Y. Pei, and Z. Ren, Mater. Today Phys. **2**, 54 (2017).